In-Situ Erosion Monitoring for Plasma Thrusters

IEPC-2024-533

Presented at the 38th International Electric Propulsion Conference
Pierre Baudis Convention Center • Toulouse, France
June 23-28, 2024

Ivan Romadanov[1]
Princeton Plasma Physics Laboratory, Princeton, NJ 08543, USA

Matthieu Couturier [2]
École Polytechnique, Palaiseau, 91120, France

Ishaan Mishra[3]
Rose-Hulman Institute of Technology, Terre Haute, Indiana, 47803, USA

Jacob Kiviat[4]
Cornell University, Ithaca, NY, 14853, USA

and

Yevgeny Raitses[5]
Princeton Plasma Physics Laboratory, Princeton, NJ 08543, USA

Abstract: In this work, we present the development and implementation of a high-resolution optical diagnostic system designed for in situ monitoring and measurement of wall erosion in electric propulsion devices, particularly Hall thrusters. The diagnostic system is based on a refined Long-Distance Microscope (LDM) system, positioned externally to simplify operations within the vacuum chamber. The LDM leverages an enhanced Shape-From-Focus (SFF) algorithm, incorporating a fitting function to improve depth resolution. This diagnostic was validated through comparative analysis with confocal microscopy, which served as a ground truth. Initial tests and validation confirmed the achievable resolutions of ~30 µm from a distance exceeding 1 meter.

Nomenclature

BCA	=	*Binary Collision Approximation*
SFF	=	*shape from focus*
BN	=	*boron nitride*
DOF	=	*depth of focus*
LDM	=	*Long-Distance Microscope*
WD	=	*Working Distance*
L	=	*LDM range of motion*
λ	=	*wavelength*
n	=	*index of refraction*

[1] Associate research physicist, Applied Materials and Sustainability Sciences, iromada2@ppp.gov
[2] Graduate student, PPPL internship, matthieu.couturier@polytechnique.edu
[3] Undergraduate, PPPL internship, mishrai@rose-hulman.edu
[4] Graduate student, PPPL internship, jak482@cornell.edu
[5] Principal Research Physicist, Discovery Plasma Science, yraitses@pppl.gov

NA = *numerical aperture*
Y_n = *sputter yield at normal angle of incidence*
θ = *ion incidence angle*

I.Introduction

The progress of space missions is increasingly reliant on accurately predicting the performance and lifetime of high-power electric propulsion (EP) systems. With the space industry evolving towards longer service times in orbit and enhanced thruster power[1], the need for efficient ground testing strategies is becoming more crucial. A key strategy in this regard is accelerated testing, designed to predict thruster lifetimes within shorter periods, thus offering significant cost and time efficiencies in thruster development. However, implementing this approach poses challenges, primarily due to the complexity involved in simulating the actual operational conditions of thrusters and a lack of reliable predictive erosion models. Although recent progress in plasma-wall interaction models and material databases offers promising insights, their predictive accuracy with application to plasma thrusters remains limited[2]. Traditional validation methods, involving extensive thruster operations that replicate real-life conditions, are both costly and time-consuming[3]. An alternative strategy involves operating the thruster under elevated power regimes to accelerate aging, which is effective only if these conditions do not alter fundamental aging mechanisms. Understanding these mechanisms and developing relevant physical models and scaling laws are crucial to guide this accelerated approach. To address these challenges, an alternative accelerated testing approach was proposed by Raitses and Keidar in which the thruster channel is designed to have enhanced erosion by sputtering under nominal (or designed) operating conditions [4,5]. This is achieved by modifying part of the channel wall geometry to optimize the ion incidence angle, thereby maximizing io-induced sputtering, while preserving the fundamental erosion mechanisms. The rationale behind this approach is the known dependency of the sputtering yield on the ion incidence angle, which follows an approximate $cos^{-1}(\theta)$ relationship[6]. In Hall thrusters, the incidence angle varies along the channel.

Typically, in aged channels, this angle is about $30-40^o$ relative to the original wall. By redesigning the channel walls to maintain an incidence angle of around $70-80^o$, the significant increase in the erosion rate is expected, thereby providing an accelerated testing method for Hall thrusters, which typically feature ceramic channels. However, even in such accelerated strategies, the challenge is still how to measure the erosion rate of the thruster channel walls in situ and in real time with sufficiently small-time step to characterize their evolution during the thruster operation desirable without stopping the thruster operation and without its exposure to the air.

Existing diagnostic methods, including in-situ laser holography[7] and microscopy[8–10], have limitations like limited resolution and complex setup requirements. In electric propulsion, techniques such as mass change control[11], optical emission spectroscopy[12], mass spectrometry[13], laser spectroscopy[14,15], and telemicroscopy[16] have been explored. However, only telemicroscopy directly measures erosion by tracking surface morphology changes. LDMs have been utilized alongside high-speed cameras for imaging electrospray thruster emissions[10]. Additionally, in-situ thermal characterization of ion thruster grids using a pyrometer has been demonstrated[8], where LDMs or telemicroscopes image grid holes to measure their sizes. LDM imaging has also been employed to qualitatively validate erosion values derived from Triangular Laser Head measurements[16]. In Sitael's Advanced Electric Propulsion Diagnostic system[9], an LDM combined with a laser system illuminates the surface with a narrow band of light. The setup, built at PPPL, utilizes only LDM without need for other optical components (e.g. lasers) and enables the measurement of erosion-induced changes in surface structure, as observed through images captured by the LDM.

In this work, we present recent progress in development of a diagnostic tool located outside the vacuum chamber, designed for continuous, in-situ monitoring of erosion. Outside location allows for uninterrupted test and ease requirements for vacuum compatibility of measurement system, but what is more important, there is no need for thermal management and protection from plasma supporting of diagnostic components as compared to systems where diagnostic was located inside[17]. The goal is to achieve high resolution of surface features, allowing for the detection of surface variations due to erosion at any stage of the thruster operation and during short test (hours) periods. The ability to detect variations in surface morphology during any stage of the thruster operation is crucial for understanding the underlying physics, e.g. erosion of previously unexposed to the plasma wall can be significantly different from wall erosion after extended operation. Real-time erosion measurements provide valuable data essential for refining erosion models. Placing the tool outside the vacuum chamber ensures uniform testing conditions and eliminates disruptions caused by intermittent sample removal.

The diagnostic core is a long-distance microscope (LDM), integrated with a shape-from-focus (SFF) [17–19], algorithm. Here, we report initial results of measurements of uneroded target geometry and verification of these measurements with a high-resolution confocal microscopy. The reported limit of feature detection is approximately

30μm over the distance of 1m, which is only an order of magnitude larger than the diffraction limited resolution (~ 4 μm) of the system (see Eq. 1). For example, initial estimates indicate that with a 350 eV Xe ion flow at an angle optimized for erosion, an erosion depth of approximately 30μm could be observed after about 4 hours of operation.

Initial tests used a Boron -Nitride (BN) target, designed to enhance erosion rates, and a 3 cm Kaufman-type gridded ion source producing a 600 eV neutralized Argon ion beam. Estimating erosion time as $t = \Delta z/JY$ with Y being the sputtering yield in mm^3/C, J the current and Δz the erosion, yields 6 hours of operation for an erosion depth of 30 μm.

This paper is structured as follows: Section II details of the diagnostic tool, data collection and processing algorithm, and design of the BN target. Section III outlines the experimental setup. Section IV presents the LDM results together with verification results from the confocal microscopy. Finally, Section V concludes the paper.

II.Approach

An accelerated life test has been designed to expedite the study of erosion in Hall thruster channel walls, focusing particularly on high-wear areas and the influence of operational parameters. The optimization of the ion incidence angle on the channel walls is achieved by introducing grooves into the ceramic walls, configured as right triangles with the hypotenuse oriented towards the anode, as shown in Fig. 1. These grooves (1-2 mm in size) are located near the channel exit at the ionization and acceleration regions where erosion is strongest[20,21]. The anticipated increase in erosion on the wall facing the anode is attributed to the dependence of the erosion yield on the angle of incidence, which follows a ~(cosθ)^(-1) relationship[22]. By adjusting the angles of these grooves on both the outer and inner walls of the channel, control over the erosion rates is achieved.

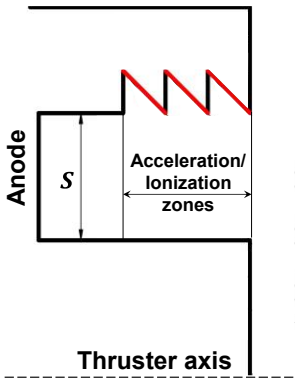

Figure 1. Schematic of the proposed ceramic wall modification (not to scale, inner wall grooves are not shown). Surfaces marked with red will have the maximum erosion rate.

In the experiments outlined in this paper, a BN target was employed to emulate the simplified geometry and materials typical of Hall thruster walls. This target, integrated with grooves strategically designed to enhance erosion rates, was conceived through theoretical modeling and binary collision simulations. Comprehensive details regarding the target design, simulations, and theoretical modeling are discussed in the following sections.

A. Diagnostic Tool

LDM, integrated with the Shape-From-Focus (SFF) image processing algorithm, is employed for real-time, in-situ monitoring of surface erosion or material deposition[17]. SFF method is based on continuous adjustment of camera's focus position, capturing a sequence of images at varied focal planes as the LDM is stepwise moved towards the object. In this sequence, each collected image has different regions of the object in focus, while the rest of the image is blurred. The depth map is constructed by determining the LDM position at which the focus measure for each pixel or region reaches its peak, thereby generating a high-resolution topography map (a 2D matrix denoting the LDM positions at which corresponding pixels are most in-focus, based on selected focus measure function and its fit, as will be explained below). This facilitates accurate measurements of surface features and microstructures. The resolution of LDM systems, contingent on optical quality and camera sensor type, can theoretically approach as low as single μm, constrained by the system's diffraction limit. Important consideration for the resolution of the system is the wavelength at which images are collected, as depth of focus (DOF) is

$$DOF = \frac{\lambda\sqrt{n^2 - NA^2}}{NA^2}, \quad (1)$$

The 38th International Electric Propulsion Conference, P. Baudis Convention Center, Toulouse, France June 23-28, 2024

where λ is the wavelength, $NA = nD/2f$ is the numerical aperture of the optical setup, n is the index of refraction, D is the optics diameter, and f is the focal distance. Thus, collection at shorter wavelength results in narrower in-focus region and higher resolution of the system. Light source centered at 415 nm was utilized in this study. Simple estimations for current system with $D = 10$ cm and $f = 100$ cm, give approximate $DOF \sim 4\mu m$. This is a theoretical limit for the resolution of LDM system at this distance.

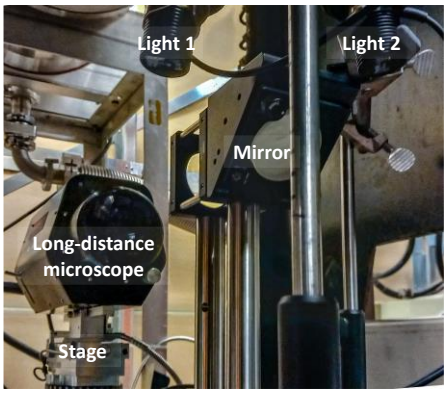

Figure 2. LDM optical setup with the Velmex stage. Camera is not shown.

The PPPL optical platform for in-situ erosion measurements is engineered to provide vibration protection and high reliability. It features a modified LDM setup, based on the designs by Ottaviano et al.[17], with the optical system and image collection moved outside of the vacuum chamber while preserving resolution. This setup includes a Questar QM 1 MK III LDM, a Maksutov Cassegrain Catadioptric microscope capable of working distances up to 1.6 m, achieving a depth of focus (DOF) of 950 µm. A Velmex motorized stage offers precise control with a 6-inch range and a step size of 1.6 µm, maintaining a movement speed up to 1.5 mm per second. Vibration isolation is ensured by mounting the assembly on a specialized platform. Imaging is done with an Allied Vision Alvium 1800 U-500c camera, featuring a 5.0 MP sensor. The target is imaged through a mirror system via a viewport in the vacuum chamber, as depicted in Fig. 2. The Thorlabs M415L4 collimated LED lights, emitting at 415±14 nm, serve as the light source for imaging. As compared to our previous LDM setup reported in [5], the second light source was installed to enable in-situ measurements while having the whole diagnostic setup outside of the vacuum chamber volume.

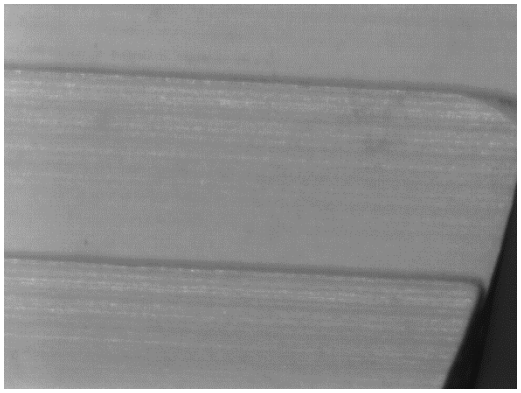

Figure 3. Example of target image collected by LDM without post-processing.

B. Data Collection and Processing

The Shape From Focus algorithm by Nayar et al.[18] generates surface depth maps using images from an LDM, which incrementally moves towards the target. Each step focuses on different parts of the object. The setup includes a semi-automated focus finder that accurately determines the starting position, defined when the target's central region is in focus. This algorithm calculates the focus measure at the target's center as a function of the LDM position and fits it with a Gaussian distribution to define the optimal focus. Scanning covers a range of 4-6 mm around the optimal focus position, with 10-30 µm steps. The Thorlabs M415L4 collimated LED light, emitting at 415±18 nm, serves as the light source for imaging, utilizing shorter wavelengths for enhanced clarity. An unprocessed image sample is shown in Fig. 3.

The SFF procedure comprises a pre-processing step and a depth calculation phase. During pre-processing, images are loaded along with their respective depths and are algorithmically aligned with respect to the first image to correct for mechanical imperfections of the moving stage. Noise reduction is achieved by smoothing the images, which can be optionally downscaled to expedite computational processes. In the subsequent depth calculation step, a focus score map, derived from various metrics[17] is applied to each image in the batch. Here, the focus score for each pixel, as a function of depth, is maximized. It will be shown later that the maximum resolution attainable is approximately 25 µm; therefore, we perform windowed averaging of the focus scores over frames of this dimension and fit a Gaussian function to the aggregated data points. The maximum of this function determines the

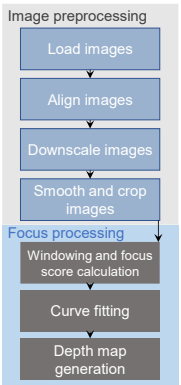

Figure 4. Image processing algorithm.

The 38th International Electric Propulsion Conference, P. Baudis Convention Center, Toulouse, France June 23-28, 2024

location of best focus for this region. This process results in the generation of a composite image, which consists of a superposition of all pixels in focus, accompanied by their height profiles. For enhanced performance, the processing algorithm is designed to run on parallel computing architectures, with improved memory management implemented during the loading phase. This process uses a modified algorithm introduced by Ottaviano et al., detailed in Fig. 4.

One of the significant improvements as compared to our previous work is implementation of focus measure fitting. Rather than determining the depth of a given point by identifying the maximum of its focus measure, a Gaussian curve is fitted to its focus measurements, with the mean of this curve representing the depth. The Gaussian function is defined as $G_{\{k,\mu,\sigma,d\}}(x) = ke^{-(x-\mu)^2/2\sigma^2} + d$, where k is the amplitude, μ is the best "in focus" position, σ is the width of "in focus" region, and d is the offset signal. To improve noise characteristics of the focus measure function it is averaged over a window of 25 μm characteristic size, as discussed before. The standard deviation is calculated from $\int \mathcal{G}_{k,\mu,\sigma,0} = \sigma k\sqrt{2\pi}$, achieved through numerical integration. The remaining fitting parameter is μ, which is determined using a least-squares method, specifically MATLAB's built-in fminsearch function. While fitting for the standard deviation is feasible, it tends to reduce the stability of the method. Example of the experimentally obtained focus measure and corresponding Gaussian fit is shown in Fig. 5. One can see that location of the "best" focus position is refined by utilizing fitting algorithm, that results in better depth reconstruction.

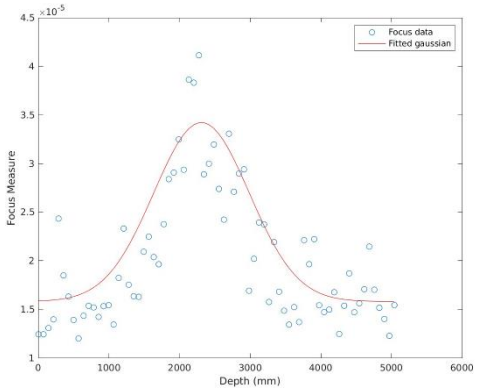

Figure 5. Example of focus measure fitting for 25 μm x 25 μm window.

III.Experimental setup

Design of the BN target and description of experimental setup along with the data collection system are presented in this section.

C. Design of boron nitride target

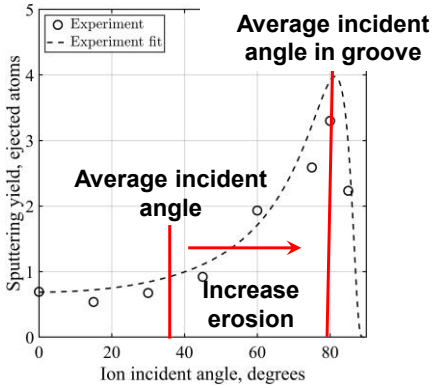

Figure 6. Sputter yield as a function of ion incident angle for experimental data.

In the experiments outlined in this document, an h-BN ceramic target was crafted to maximize erosion rates and to facilitate observable surface alterations during plasma operations. Binary Collision Approximation (BCA) [23] simulations, specifically utilizing the TRIM software, a Monte Carlo-based BCA tool, informed the target design. TRIM evaluates the angular dependence of ion incidence on sputter yield by randomly distributing target atoms according to the target's density. Our aim was to identify the angle of incidence that would yield the highest sputter rates. This angle was determined by correlating results from TRIM simulations with experimental data from Chen et al.[24]and by applying Yamamura's semi-empirical model[6] to this data. This model is

$$Y_\theta = Y_n \cos^{-F}(\theta) e^{G} \quad (2)$$

Experimental data were gathered using 810 eV Argon ions on h-BN[24], and the model was validated against this dataset. To match the experimental results with TRIM simulations, the data at 810 eV were linearly scaled down to 600 eV, reflecting the linear relationship between the incident ion energy and the sputter yield within this specific energy range. This scaling addresses the complexities involved in predicting sputtering for BN, given its regular crystal structure and the variability in parameters such as surface binding energy. The findings are illustrated in Fig. 6, where red lines represent averaged incident angles for both regular and grooved geometries, showing a sputtering yield increase by approximately 4 times.

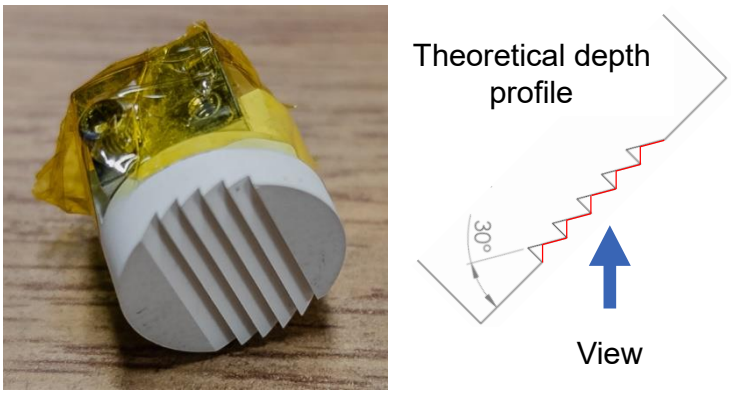

Figure 7. Photo of the designed target for accelerated erosion tests and theoretical depth profile.

Based on these estimations, a target was designed such that the angle of incidence of an ion beam with the surface is 75°. Target photo and theoretical depth profile as viewed by the LDM are presented in Fig. 7.

D. Vacuum facility and general setup overview

The general schematic of the experimental setup is depicted in Fig. 8. The Small Hall Thruster Facility (SHTF) [25] comprises a vacuum vessel, which includes gas supply systems and power supplies. The vessel itself is constructed from stainless steel and measures 1 m in length and 0.8 m in diameter. Vacuum conditions are achieved using a combination of a blower, a mechanical pump, and an Osaka TG3203M turbo-molecular pump, which result in a base vacuum pressure of $\sim 6 \cdot 10^{-6}\ Torr$. Argon gas flow is regulated by a mass flow controller with 0 to 10 sccm range. During operation the background gas pressure, adjusted for argon, is maintained below $6 \cdot 10^{-5}\ Torr$. Pressure is monitored using an external ion gauge mounted on the top of the vacuum chamber.

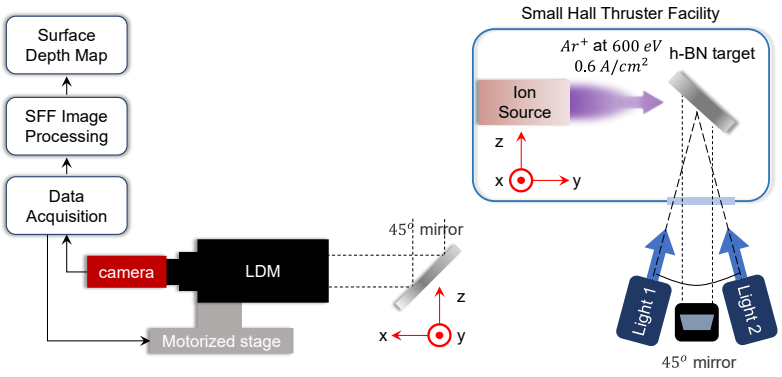

Figure 8. General schematic of the experimental setup.

A 3-cm Kaufman-type gridded ion source is utilized to generate an Argon plasma and accelerate the Ar+ ions over a 600 V potential difference within the SHTF. The tungsten filament neutralizer, integrated into the ion source for emitting electrons to neutralize the ion beam, also serves as the light source for the h-BN target. The operating ion source and BN target are depicted in Fig. 8. Ion beam current at the target position was measured with specifically designed planar probe of 1.8 cm^2 area and at 5 sccm current density was 0.6 mA/cm^2

E. Data acquisition

Data acquisition and motion control are facilitated through the integration of a Raspberry Pi 4B, a RedPitaya STEMLab 125-14, and a motor controller. All functionalities, including motor movement, image acquisition, and encoder signal processing, are managed by a Python script running on the Raspberry Pi. It records the distances traveled during each motor movement, which are essential for correlating with depth map data obtained via the SFF algorithm. The RedPitaya functions as a DAQ for capturing encoder signals and sends trigger signals for the motor controller. The Raspberry Pi is also communicating with the camera responsible for capturing surface images. The operational workflow of this system is outlined in Fig. 9. At the beginning, the linear stage is centered, and the image scanning process starts from $x = -L/2$ to $x = L/2$ with a preset step size.

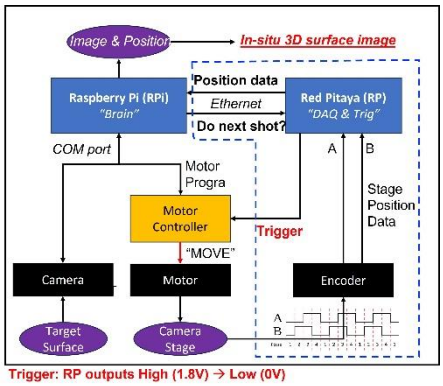

Figure 9. Flow chart of the system for LDM operations.

The 38th International Electric Propulsion Conference, P. Baudis Convention Center, Toulouse, France June 23-28, 2024

F. Confocal microscopy

We aim to evaluate the accuracy of our SFF algorithm by comparing it against a ground truth. For this purpose, a 0.6x0.6 mm region near one of the ridges is imaged using Keyence VK-X3050 confocal microscope[26] that has a vertical accuracy of ±5 nm and a 630 nm per pixel resolution at 20x magnification. Example of the imaged region is shown in Fig 10. The focus of our comparison is on the surface details captured by confocal microscopy relative to those from LDM measurements.

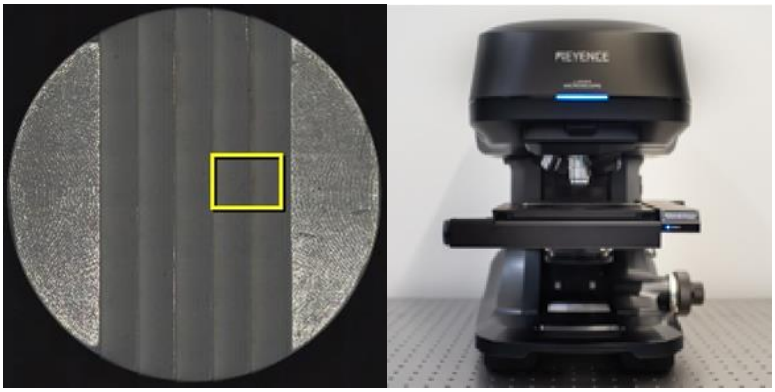

Figure 10. Confocal microscopy image and setup.

IV.Conclusion

Measurements before target exposure to the ion beam are presented in Fig. 11. The SFF algorithm-generated heightmap, without fitting of the focus measures, is depicted in Fig. 11a. This reconstructed surface was averaged along the X-axis, and the surface roughness of the resulting profile was estimated by the standard deviation of the difference between the flat central part of the profile and its linear fit (see red line in Fig. 11). Both profiles, aligned for overlap, demonstrate close resemblance, although end regions were trimmed to avoid errors from optics vignetting. The difference between the measured and CAD profiles was refined as surface roughness and was quantified by taking a standard deviation of their difference, yielding δ_{before}=58 μm.

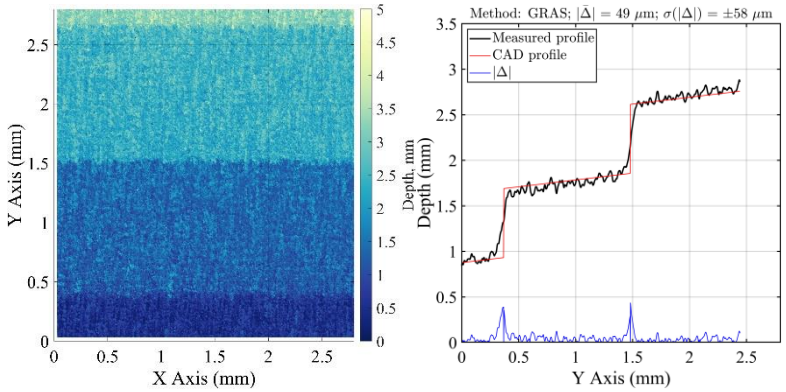

Figure 11. Depth map obtained with SFF. Depth map profiles: SFF algorithm(black), linear fit (red), and their difference.

The impact of the fitting process is illustrated in Fig. 12, where the surface profile is derived from the depth map, with depth determined by the location of the peak of the fitted Gaussian function. CAD surface profile is shown in blue. Note, that this is the same location, as shown in Fig 11, but different dataset, thus, there is a difference in shown profiles. This method significantly enhances the determined surface roughness, achieving an improved resolution of $\delta_{before} = 29\ \mu m$, effectively doubling the previously attainable resolution.

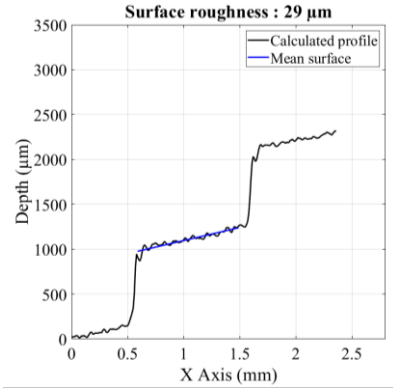

Figure 12. Depth map profiles with Gaussian fitting

Finally, to verify resolution of LDM, it is compared with confocal microscope results. Comparison was performed by analysis of the detectable spatial frequencies (mm^{-1}) by both methods. Despite the horizontal resolution of the LDM images being comparable to that of confocal microscopy (ranging from 1.6 to 2.0 μm at distances of 106 to 132 cm), the primary constraint lies in the resolution degradation caused by the SFF algorithm.

A comparison of spatial frequencies was conducted for profiles averaged along the X-direction from both confocal and LDM depth maps. Cross-coherence analysis was employed to identify common frequencies between the two

methods. The resulting cross-coherence plot, shown in Fig. 14, reveals peaks at spatial frequencies of 5, 15, 35, and 45 mm^{-1}. Coherence at these frequencies indicates significant correlations between two methods, demonstrating that both methods capture common patterns at these scales. Thus, LDM resolution can be estimated as 22 μm ($1/45mm^{-1}$).

After ion beam exposure measurements (~1.5 hours) are illustrated in Fig. 15. The post-exposure profile appears noisier, with a surface roughness of $\delta_{after} = 120\ \mu m$. While there is a difference between δ_{before} and δ_{after}, this difference is still within the errorbars and experiments with longer exposure times are required.

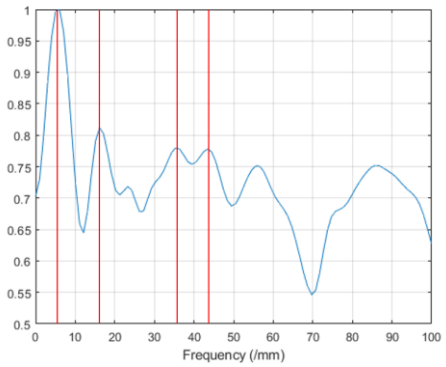

Figure 13. Cross-coherence of LDM and confocal methods. Red circles mark most prominent frequencies

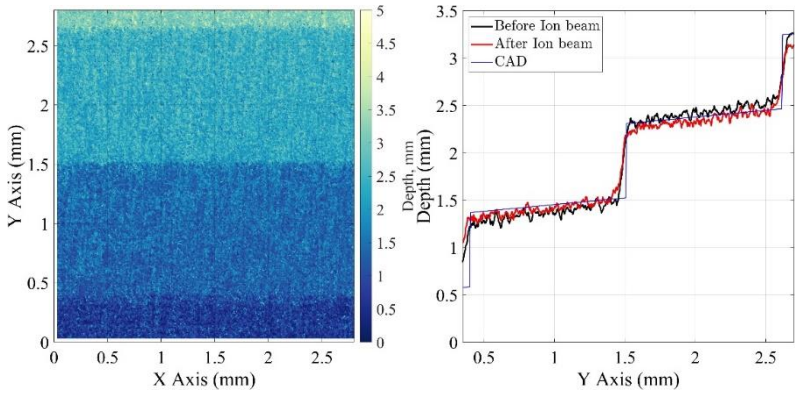

Figure 14. Depth map after plasma exposure. Comparison of depth map profiles before and after plasma exposure.

V.Conclusion

Addressing the challenges of lifetime and wear tests in Hall thrusters, this study explores an accelerated erosion test strategy that leverages the angular dependence of ion-induced sputtering yield to enhance the erosion of channel walls with modified geometry. The main focus of this research was the further development and validation of a previously established in-situ diagnostic, which will be used to monitor such accelerated erosion, based on the LDM approach. Significant improvements were made to the SFF algorithm by integrating a fitting function for the focus measure parameter, which enhanced the achievable depth resolution to ~30 µm at a distance of 1 m. Such resolution enables the detection of erosion on BN surfaces after about 6 hours of continuous operation. This adjustment also has the potential to reduce the number of images required per measurement, as the in-focus position of pixels can now be determined from the fitted curve. The diagnostic method was validated against the confocal microscopy technique, which offers superior resolution and serves as a ground truth. By comparing the spatial frequencies prominent in both methods, the resolution of the LDM approach was determined to be 22 µm. Future steps include improving measurement resolution through machine learning methods and adapting the LDM system for experiments with a 2 kW Hall thruster operated using Xe, Kr, N2, and air as propellants[27].

Acknowledgments

This work was supported by AFOSR grant. IM and JK were supported by Summer Undergraduate Laboratory Internship (SULI) program of the US Department of Energy. Authors would like to acknowledge Prof. M. Keidar for fruitful discussions.

References

[1] Peterson, P., Jacobson, D., Manzella, D., and John, J., "The Performance and Wear Characterization of a High-Power High-Isp NASA Hall Thruster," presented at the 41st AIAA/ASME/SAE/ASEE Joint Propulsion Conference & Exhibit, Tucson, Arizona, 2005. https://doi.org/10.2514/6.2005-4243

[2] Garrigues, L., Boniface, C., Hagelaar, G. J. M., Boeuf, J. P., and Duchemin, O., "Performance Modeling of a Thrust Vectoring Device for Hall Effect Thrusters," *Journal of Propulsion and Power*, Vol. 25, No. 5, 2009, pp. 1003–1012. https://doi.org/10.2514/1.39680

[3] de Grys, K., Mathers, A., Welander, B., and Khayms, V., "Demonstration of 10,400 Hours of Operation on 4.5 kW Qualification Model Hall Thruster," *46th AIAA/ASME/SAE/ASEE Joint Propulsion Conference & Exhibit*, American Institute of Aeronautics and Astronautics, 2010. https://doi.org/10.2514/6.2010-6698

[4] Keidar, M., and Raitses, Y., "Enhancement of the Channel Wall Erosion with Application to Accelerated Testing of Hall Thrusters," white paper to the AFOSR (unpublished), 2022.

[5] Romadanov, I., Mishra, I., Kiviat, J., Son, S. H., Benjadol, B., Ottaviano, A., Raitses, Y., and Keidar, M., "In-Situ Diagnostic of Channel Erosion in Hall Thrusters," presented at the AIAA Sci Tech Forum, Orlando, FL, USA, 2024.

[6] Yamamura, Y., and Shindo, S., "An Empirical Formula for Angular Dependence of Sputtering Yields," *Radiation Effects*, Vol. 80, Nos. 1–2, 1984, pp. 57–72. https://doi.org/10.1080/00337578408222489

[7] Thomas, C. E. (Tommy), Granstedt, E. M., Biewer, T. M., Baylor, L. R., Combs, S. K., Meitner, S. J., Hillis, D. L., Majeski, R., and Kaita, R., "Digital Holography for *in Situ* Real-Time Measurement of Plasma-Facing-Component Erosion," *Review of Scientific Instruments*, Vol. 85, No. 11, 2014, p. 11D810. https://doi.org/10.1063/1.4886435

[8] Bundesmann, C., Tartz, M., Scholze, F., Neumann, H., Leiter, H. J., and Scortecci, F., "In Situ Thermal Characterization of the Accelerator Grid of an Ion Thruster," *Journal of Propulsion and Power*, Vol. 27, No. 3, 2011, pp. 532–537. https://doi.org/10.2514/1.50049

[9] Andreussi, T., Pieri, L., Albertoni, R., and Andrenucci, M., "Telemicroscopy Erosion Measurements of 5 kW-Class Hall Effect Thruster Channel Walls IEPC-2015-348 / ISTS-2015-b-348," 2015.

[10] Wirz, R. E., "Electrospray Thruster Performance and Lifetime Investigation for the LISA Mission," *AIAA Propulsion and Energy 2019 Forum*, American Institute of Aeronautics and Astronautics, 2019. https://doi.org/10.2514/6.2019-3816

[11] Basak, D., Noushkam, N., Glogowski, M., Crofton, M. W., and Young, J. A., "Sputtering Effects of Xenon Ion Thruster Plume on Common Spacecraft Materials," *AIAA SPACE 2015 Conference and Exposition*, American Institute of Aeronautics and Astronautics, 2015. https://doi.org/10.2514/6.2015-4642

[12] Celik, M., Batishchev, O., and Martinez-Sanchez, M., "Use of Emission Spectroscopy for Real-Time Assessment of Relative Wall Erosion Rate of BHT-200 Hall Thruster for Various Regimes of Operation," *Vacuum*, Vol. 84, No. 9, 2010, pp. 1085–1091. https://doi.org/10.1016/j.vacuum.2010.01.031

[13] King, L. B., "Transport-Property and Mass Spectral Measurements in the Plasma Exhaust Plume of a Hall-Effect Space Propulsion System," Ph.D. University of Michigan, United States -- Michigan.

[14] Duan, X., Guo, D., Cheng, M., Yang, X., and Guo, N., "Measurements of Channel Erosion of Hall Thrusters by Laser-Induced Fluorescence," *Journal of Applied Physics*, Vol. 128, No. 18, 2020, p. 183301. https://doi.org/10.1063/5.0020074

[15] Lee, B. C., Huang, W., Tao, L., Yamamoto, N., Gallimore, A. D., and Yalin, A. P., "A Cavity Ring-down Spectroscopy Sensor for Real-Time Hall Thruster Erosion Measurements," *Review of Scientific Instruments*, Vol. 85, No. 5, 2014, p. 053111. https://doi.org/10.1063/1.4879135

[16] Bundesmann, C., Eichhorn, C., Neumann, H., Scholze, F., Spemann, D., Tartz, M., Leiter, H. J., Gnizdor, R. Y., and Scortecci, F., "In Situ Erosion Measurement Tools for Electric Propulsion Thrusters: Triangular Laser Head and Telemicroscope," *EPJ Techniques and Instrumentation*, Vol. 9, No. 1, 2022, pp. 1–23. https://doi.org/10.1140/epjti/s40485-022-00076-z

[17] Ottaviano, A., Thuppul, A., Hayes, J., Dodson, C., Li, G. Z., Chen, Z., and Wirz, R. E., "*In Situ* Microscopy for Plasma Erosion of Complex Surfaces," *Review of Scientific Instruments*, Vol. 92, No. 7, 2021, p. 073701. https://doi.org/10.1063/5.0043002

[18] Nayar, S. K., and Nakagawa, Y., "Shape from Focus," *IEEE Transactions on Pattern Analysis and Machine Intelligence*, Vol. 16, No. 8, 1994, pp. 824–831. https://doi.org/10.1109/34.308479

[19] Billiot, B., Cointault, F., Journaux, L., Simon, J.-C., and Gouton, P., "3D Image Acquisition System Based on Shape from Focus Technique," *Sensors*, Vol. 13, No. 4, 2013, pp. 5040–5053. https://doi.org/10.3390/s130405040

[20] Burton, T., Schinder, A. M., Capuano, G., Rimoli, J. J., Walker, M. L. R., and Thompson, G. B., "Plasma-Induced Erosion on Ceramic Wall Structures in Hall-Effect Thrusters," *Journal of Propulsion and Power*, Vol. 30, No. 3, 2014, pp. 690–695. https://doi.org/10.2514/1.B34882

[21] Zidar, D. G., and Rovey, J. L., "Hall-Effect Thruster Channel Surface Properties Investigation," *Journal of Propulsion and Power*, Vol. 28, No. 2, 2012, pp. 334–343. https://doi.org/10.2514/1.B34312

[22] Murty, M. V. R., "Sputtering: The Material Erosion Tool," *Surface Science*, Vol. 500, Nos. 1–3, 2002, pp. 523–544. https://doi.org/10.1016/S0039-6028(01)01586-2

[23] Ziegler, J. F., and Biersack, J. P., "The Stopping and Range of Ions in Matter," *Treatise on Heavy-Ion Science: Volume 6: Astrophysics, Chemistry, and Condensed Matter*, edited by D. A. Bromley, Springer US, Boston, MA, 1985, pp. 93–129. https://doi.org/10.1007/978-1-4615-8103-1_3

[24] Meng Chen, Rohrbach, C., Neuffer, A., Barth, K.-L., and Lunk, A., "Simulation of Boron Nitride Sputtering Process and Its Comparison with Experimental Data," *IEEE Transactions on Plasma Science*, Vol. 26, No. 6, 1998, pp. 1713–1717. https://doi.org/10.1109/27.747890
[25] Smirnov, A., Raitses, Y., and Fisch, N. J., "Plasma Measurements in a 100 W Cylindrical Hall Thruster," *Journal of Applied Physics*, Vol. 95, No. 5, 2004, pp. 2283–2292. https://doi.org/10.1063/1.1642734
[26] "Measurement Head - VK-X3050 | KEYENCE America." Retrieved 19 June 2024. https://www.keyence.com/products/microscope/laser-microscope/vk-x3000/models/vk-x3050/
[27] Raitses, Y., Staack, D., Dunaevsky, A., Dorf, L., and Fisch, N., "Measurements of Plasma Flow in a 2 kW Segmented Electrode Hall Thruster," presented at the the 28th International Electric Propulsion Conference, Toulouse, France, 2003.